

37th AIAA Plasmadynamics and Lasers Conference, 5-8 June 2006, San Francisco, California

# Modeling of Dielectric Barrier Discharge Plasma Actuator with Atmospheric Air Chemistry

K.P. Singh\*, Subrata Roy†

*Computational Plasma Dynamics Laboratory  
Mechanical Engineering, Kettering University  
Flint, MI 48504, USA*

Datta V. Gaitonde‡

*Computational Sciences Branch  
Air Force Research Laboratory  
Wright Pat AFB, Ohio 45433, USA*

Surface discharge in air has been studied using chemistry of formation of different ion and neutral species of nitrogen and oxygen. Continuity equations governing densities of electrons, ions and neutral species of nitrogen and oxygen are solved with Poisson's equation to obtain spatial and temporal profiles of densities, and voltage. Results show that density profiles of charged species are nearly opposite to each other about the electrode set at positive and negative peaks of the cycle. Density profiles of nitrogen atom N and oxygen atom O are similar to each other at the same temporal location in a cycle because these do not respond to the electric field. Also  $N_2^+$  and  $O_2^+$  respond to electric field in a similar manner, hence, their density profiles are similar to each other at same time instance. There is difference in the level of ionization of different species due to difference in rate coefficients. The motion of electrons and ions in response to electric field results in charge separation. The value of separated space charge shows footprints of electron deposition downstream of the overlap region of the electrodes resulting in formation of virtual negative electrode. The electrodynamic body force per unit volume has been predicted about the dielectric surface for the twentieth cycle. A time averaged force, predominantly downstream with a transverse component towards the wall, acts on the plasma in forward direction. This results in a moving wave of plasma over dielectric surface in the positive x-direction which can induce a control mechanism in the neighboring air flow.

## Nomenclature

D	Diffusion coefficient, $\text{cm}^2/\text{s}$	O	Oxygen atom
E	Electric field, $\text{V}/\text{cm}$	$O_2^+$	Positive oxygen ion
e	Electron charge, statcoulomb	$O^-$	Negative oxygen ion
$\epsilon$	Permittivity, farad/m	$\omega$	Applied frequency, radians
<b>F</b>	Electric force density, $\text{dynes}/\text{cm}^3$ , $\mu\text{N}/\text{cm}^3$	P	Pressure, Pa
$\phi$	Potential, V	q	Charge separation, statcoulomb
K	Rate coefficients, $\text{cm}^3 \text{s}^{-1}$	T	Time coordinate, s
$k_B$	Boltzmann constant	t	Temperature, eV
L	Electrode length, cm	<b>V</b>	Velocity, m/s
$\lambda_D$	Electron Debye length, cm	X	Spatial coordinate, cm
M	mass, kg		
$\mu$	Mobility, $\text{cm}^2 \text{V}^{-1} \text{s}^{-1}$	Subscript	
N	Number density, $\text{cm}^{-3}$	s:	
$N_2$	Nitrogen molecule	$\alpha$	Species
N	Nitrogen atom	B	Boltzmann
$N_2^+$	Positive nitrogen ion	E	Electron, finite element
$O_2$	Oxygen molecule	I	Ion
		N	Neutral

\* Post Doctoral Research Associate of the CPDL, 1700 West Third Avenue.

† Associate Professor of Mechanical Engineering, 1700 West Third Avenue, and AIAA Associate Fellow.

‡ Technical Area Leader, Air Vehicles Directorate/VAAC, 2210 8<sup>th</sup> St., and AIAA Associate Fellow.

# Report Documentation Page

Form Approved  
OMB No. 0704-0188

Public reporting burden for the collection of information is estimated to average 1 hour per response, including the time for reviewing instructions, searching existing data sources, gathering and maintaining the data needed, and completing and reviewing the collection of information. Send comments regarding this burden estimate or any other aspect of this collection of information, including suggestions for reducing this burden, to Washington Headquarters Services, Directorate for Information Operations and Reports, 1215 Jefferson Davis Highway, Suite 1204, Arlington VA 22202-4302. Respondents should be aware that notwithstanding any other provision of law, no person shall be subject to a penalty for failing to comply with a collection of information if it does not display a currently valid OMB control number.

1. REPORT DATE <b>JUN 2006</b>		2. REPORT TYPE		3. DATES COVERED <b>00-00-2006 to 00-00-2006</b>	
4. TITLE AND SUBTITLE <b>Modeling of Dielectric Barrier Discharge Plasma Actuator with Atmospheric Air Chemistry</b>				5a. CONTRACT NUMBER	
				5b. GRANT NUMBER	
				5c. PROGRAM ELEMENT NUMBER	
6. AUTHOR(S)				5d. PROJECT NUMBER	
				5e. TASK NUMBER	
				5f. WORK UNIT NUMBER	
7. PERFORMING ORGANIZATION NAME(S) AND ADDRESS(ES) <b>Kettering University ,Computational Plasma Dynamics Laboratory,Department of Mechanical Engineering,Flint,MI,48504</b>				8. PERFORMING ORGANIZATION REPORT NUMBER	
9. SPONSORING/MONITORING AGENCY NAME(S) AND ADDRESS(ES)				10. SPONSOR/MONITOR'S ACRONYM(S)	
				11. SPONSOR/MONITOR'S REPORT NUMBER(S)	
12. DISTRIBUTION/AVAILABILITY STATEMENT <b>Approved for public release; distribution unlimited</b>					
13. SUPPLEMENTARY NOTES					
14. ABSTRACT					
15. SUBJECT TERMS					
16. SECURITY CLASSIFICATION OF:			17. LIMITATION OF ABSTRACT	18. NUMBER OF PAGES	19a. NAME OF RESPONSIBLE PERSON
a. REPORT <b>unclassified</b>	b. ABSTRACT <b>unclassified</b>	c. THIS PAGE <b>unclassified</b>			

## I. Introduction

PLASMA actuators are useful flow control devices for various aerodynamic applications. They have been demonstrated for active mitigation of performance deficiencies under off-design conditions.<sup>1-4</sup> These actuators are distinctive for their absence of moving parts, rapid on-off deployment and attractive self-limiting characteristics. The interest of this work is in dielectric barrier discharge (DBD) driven plasma actuators operating at atmospheric pressures. DBD is widely used in applications for ozone production, surface etching, decontamination, plasma display panels, etc.<sup>2,3</sup> Typically in an atmospheric DBD, a few watts of power is supplied by a 1-50 kilovolts rms with 50 Hz to 50 kHz frequencies. The discharge is characterized as transient with a minute time scale, several orders of magnitude smaller than that for the bulk gas flow, thus allowing fast response of the fluid to the electrical impulse. The plasma actuators typically operate in air. While successful experiments<sup>1-4</sup> and simplified numerical modeling efforts<sup>5-8</sup> have prompted a tremendous interest in plasma actuators, basic first principles understanding for these devices are yet to be explored for air chemistry so that the operational limits can be further alleviated.

The applications of plasmas in hypersonic flows for sustained flight in low-pressure at upper atmosphere and during atmospheric reentry are known for physical complexity.<sup>9</sup> Severe thermal, chemical, and ionizational nonequilibrium conditions are experienced due to high velocities and high altitudes during tranatmospheric missions. The extreme environmental conditions have a major impact on the design and study of the vehicle aerodynamics and thermal loading. Chemical kinetic processes in the plasma play an important role in electromagnetic interference surrounding the craft. Knowledge of chemical kinetic processes is crucial to mission planners. The computational study has to include mass, momentum, and energy equations of the neutral species and charge particle species. The influence of the charge particles on the flow field needs to be included and the elastic and inelastic collisional energy transfer mechanisms also needs to be taken into account for the high degree of thermal, chemical and ionizational nonequilibrium in the flow field. The reactions include momentum transfer, molecular ionization, excitation, dissociation, dissociative recombination and secondary electron emission.<sup>10</sup>

The chemistry for ionized air at atmospheric pressure is even more complicated due the faster species reaction rates.<sup>10</sup> Specifically, barrier discharges in air-like  $N_2/O_2$  mixtures consist of a multitude of micro and nanoscale discharges. Theoretical modeling of these discharge processes requires a time-resolution in the subnanosecond range to describe disparate electron and ion time scales. Also, small spatial dimensions of barrier discharges at these pressures require a spatial resolution much finer than the submillimeter scale. Thus, investigation of the spatio-temporal evolution of such multiscale barrier discharge is quite a challenging but necessary task to understand the governing physics of discharge in air and in  $N_2/O_2$  mixtures. Barrier discharges offer a good technical challenge to properly understand the flow and physical models. Oxygen and nitric oxide species in the air could significantly alter the discharge due to the presence of negative oxygen ions and nitric oxide species. The negative ions add momentum in the opposite direction to the positive ions and oxygen and nitric oxide have different recombination, dissociation, and excitation behavior. In order to explore the force production differences between nitrogen, oxygen and nitric oxide, computational study needs to be carried out by including major species.

The asymmetric surface dielectric barrier discharge has been used in an experimental setup for airflow production close to the dielectric surface. Effect of several discharge parameters such as applied voltage waveform, distance between electrodes, dielectric thickness and permittivity has been experimentally determined for atmospheric pressures. The time-averaged flow velocity spatial profiles has found the wall jet velocities of up to 3.5 m/s at heights of 1–2 mm.<sup>4</sup> In another effort<sup>11</sup>, the measurements of the instantaneous flow velocity induced by surface plasma actuators in air at atmospheric pressure have been conducted with two different types of plasma actuators in order to determine the establishment time of the induced airflow. A strong correlation was found between the transient regime of the discharge current and the ionic wind velocity. The AC discharge was found to induce a pulsed airflow at a frequency corresponding to the high voltage waveform frequency and the DC discharge airflow with important fluctuations.<sup>11</sup> The performance of plasma actuators has been studied with wind tunnels, drag balances, Pitot tubes, smoke flow visualization, and fluid dynamic modeling programs. The electric power transfers the momentum to the neutral gas flow through ion-neutral collisions. The effects of actuator geometry, materials, the RF frequency and RMS voltage have been studied both experimentally<sup>3</sup> and numerically.<sup>12</sup>

The first principles modeling of the surface DBD has been reported in recent literature. A two-dimensional fluid model of the surface discharge showed the force per unit volume acting on the flow due to the momentum transfer from charged particles to neutral molecules.<sup>13</sup> The force in the DBD was found to be of the same nature as the electric wind in a corona discharge and localized in the cathode sheath region of the discharge expanding along the dielectric surface. The present authors have carried out simulation study of the dielectric barrier plasma actuator<sup>5</sup> and its effect on the mitigation of separated flows over flat plate<sup>6,12</sup> and NACA0015 airfoil<sup>14-16</sup>. They have shown that electron deposition downstream of the overlap region of the electrodes results in formation of virtual negative electrode. The force due to the charge separation is in the positive streamwise direction during most of the positive part of the rf cycle and in negative-x direction during most of the negative part of the cycle. The magnitude of the former force is higher than the latter. Thus, domain integration of the force on the charge separation and time average of the force was found primarily

to be in the positive-x and negative-y direction. In this paper, we study atmospheric air discharge using a mixture of oxygen and nitrogen about an asymmetric dielectric barrier plasma actuator. We solve the equations governing dynamics of electrons, ions and neutral nitrogen and oxygen species to obtain spatio-temporal profiles of electron density, ion density, electric potential, and neutral gas density. We identify reasons for difference in profiles of different species. The value of separated space charge and electrodynamic body force per unit volume has also been obtained for the twentieth rf cycle.

This paper is organized as follows. Section II describes the problem statement along with the air chemistry. Section III presents the computational results and relevant discussion. Section IV highlights the conclusions.

## II. Problem Statement

Fig. 1 shows schematic of an asymmetric single dielectric barrier plasma actuator. It consists of two electrodes separated by a dielectric. The upper electrode is exposed to the air while the lower electrode is placed underneath the dielectric. The region simulated is 6 cm long and 4 cm high. The lower part of the domain consists of a 0.1 cm thick insulator with dielectric constant  $\epsilon_d = a\epsilon_0$  while the upper part is filled with air of  $\epsilon_f = 1.0055\epsilon_0$ , where  $\epsilon_0$  is permittivity of the free space. We have taken  $a = 3.5$  for Kapton polyimide and negligible rf electrode thickness. The thickness of the electrodes is assumed to be infinitesimally small. The length  $L$  of both the electrodes is 2.0 mm. The rf electrode extends from  $x = 2.8$  cm to  $x = 3$  cm at  $y = 0.1$  cm, the grounded electrode is from 3.2 cm to 3.4 cm at  $y = 0$ , with a 0.2 cm gap between electrodes along the x-axis. The embedded electrode is grounded and a sinusoidal voltage  $\phi = \phi_0 \sin(2\pi ft)$  is applied to the exposed electrode. The frequency of excitation is fixed at  $f = 5$  kHz and excitation potential is  $\phi_0 = 1000$  volt.

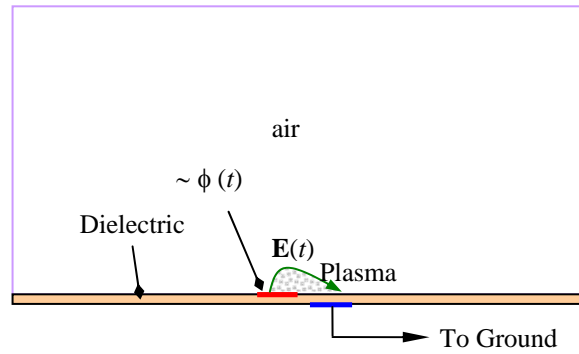


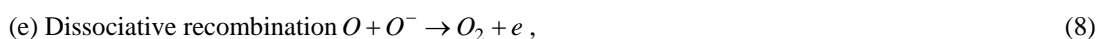
FIG. 1. Schematic of asymmetric single dielectric barrier plasma actuators operating in air.

The equations governing chemistry of discharge are as follows.<sup>10</sup> The metastable species along with  $N_4^+$  and  $O_4^+$  are neglected due to their fast recombination rates. Also, NO is not included to reduce the numerical complexity in the first principles model at this stage.

### (1) Nitrogen model



### (2) Oxygen model



The drift-diffusion form of continuity and Poisson's equations for the electrons, ions and neutrals are as follows:

$$\frac{\partial n_e}{\partial t} + \nabla \cdot (n_e \mathbf{v}_e) = k_1 n_e n_{N_2} - k_3 n_e n_{N_2^+} + (k_5 - k_7) n_e n_{O_2} + k_9 n_e n_{O_2^+}, \quad (9)$$

$$\frac{\partial n_N}{\partial t} + \nabla \cdot (n_N \mathbf{v}_N) = 2k_2 n_e n_{N_2}, \quad (10)$$

$$\frac{\partial n_{N_2}}{\partial t} + \nabla \cdot (n_{N_2} \mathbf{v}_{N_2}) = -k_1 n_e n_{N_2} - k_2 n_e n_{N_2} + k_3 n_e n_{N_2^+} \quad (11)$$

$$\frac{\partial n_{N_2^+}}{\partial t} + \nabla \cdot (n_{N_2^+} \mathbf{v}_{N_2^+}) = k_1 n_e n_{N_2} - k_3 n_e n_{N_2^+} \quad (12)$$

$$\frac{\partial n_{O_2}}{\partial t} + \nabla \cdot (n_{O_2} \mathbf{v}_{O_2}) = -(k_4 + k_5 + k_6) n_{O_2} n_e + k_7 n_{O^-} n_{O_2^+} + k_8 n_e n_{O_2^+} \quad (13)$$

$$\frac{\partial n_{O^-}}{\partial t} + \nabla \cdot (n_{O^-} \mathbf{v}_{O^-}) = (2k_5 + k_6) n_e n_{O_2} + k_7 n_{O^-} n_{O_2^+} \quad (14)$$

$$\frac{\partial n_{O_2^+}}{\partial t} + \nabla \cdot (n_{O_2^+} \mathbf{v}_{O_2^+}) = k_4 n_e n_{O_2} - k_7 n_{O^-} n_{O_2^+} - k_8 n_e n_{O_2^+} \quad (16)$$

$$\varepsilon \nabla^2 \phi = 4\pi e (n_e + n_{O^-} - n_{n_2^+} - n_{O_2^+}), \quad (17)$$

with momentum flux  $n_\alpha \mathbf{v}_\alpha = -\text{sgn}(e) n_\alpha \mu_\alpha \nabla \phi - D_\alpha \nabla n_\alpha$ , and electric field  $\mathbf{E} = -\nabla \phi$ .

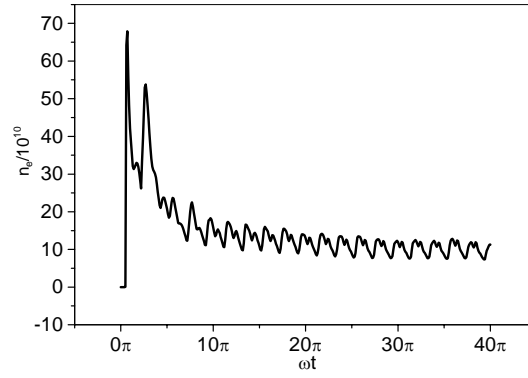
Above,  $k_1 \dots k_8$  are various rate coefficients related to Equations (1) through (8) obtained from Kossyi et al.<sup>10</sup>. Electron temperature appearing in these rate coefficients is calculated from  $\mathbf{E} = k_B T_e / \nabla n_e / n_e$ , which is obtained assuming initial Boltzmann distribution,  $n_e \propto \exp(e\phi / k_B T_e)$ . In Eqns. (9)-(17)  $n_\alpha$  and  $v_\alpha$  are density and velocities of species  $\alpha$ . The mobilities  $\mu_\alpha$  and diffusion rates  $D_\alpha$  are taken from Ellis et al.<sup>17</sup>. The bulk density of the air is taken to be  $1.3 \times 10^{-3} \text{ gm/cm}^3$ . Atmospheric ratio of 3.6 is taken for nitrogen to oxygen gas molecules. The self-consistent formulation is solved using a Galerkin variational formulation based finite-element method<sup>18</sup> to obtain electron, ion and neutral species densities of nitrogen and oxygen, and the electric potential.

Initial and boundary conditions are as follows. The all initial particle concentrations, except those of the electrons, nitrogen and oxygen molecules, are taken to be zero. Initial electron density is taken  $10^3/\text{cm}^3$ . Initial rf potential is also zero. All neutral particle concentrations are taken zero at the boundaries of the dielectric and normal components of flux are zero at outer boundaries of plasma. Normal components of electric field are taken zero on all the outer boundaries of the domain (dielectric as well as plasma domain). No electron and ion current flow inside the dielectric is considered. Electric field normal to the dielectric surface is discontinuous by the separated charge.

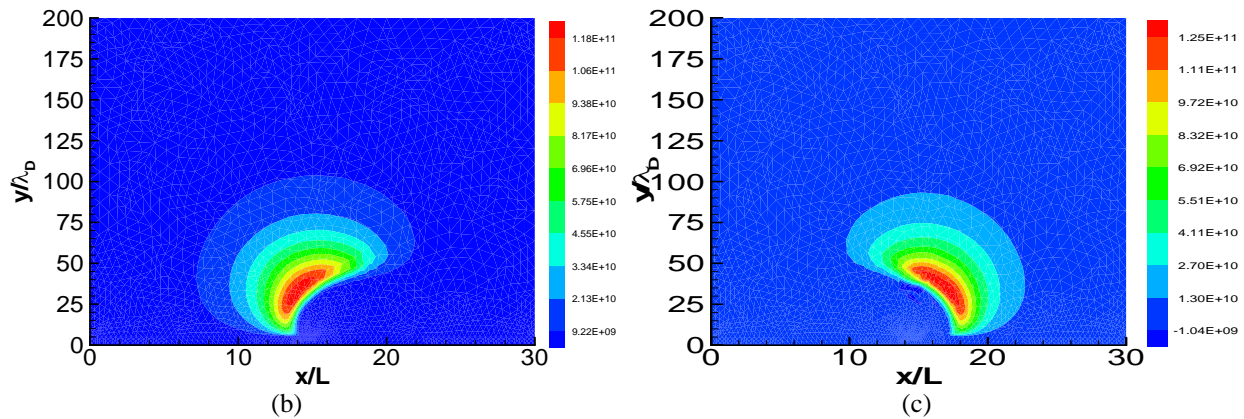
### III. Results and Discussion

As we switch on the rf voltage, discharge in the air occurs. Different ion and neutral species are formed through ionization, dissociation and dissociative attachment etc. Recombination also occurs. Full chemistry of different species formation and recombination is described by Equations (1) to (8). Figure 2 (a) shows electron density  $n_e$  as a function of normalized time  $\omega t$  for  $x/L=15$  and  $y/\lambda_D=25$ . Steady state is reached within a few cycles, thereafter; there is a small loss in the densities. as described in Figure 2a.

Initial electron density is taken  $10^3/\text{cm}^3$ . The electrons are repelled from the area of grounded electrode and are attracted towards rf electrode during positive part of the cycle. Reverse happens during negative part of the cycle, hence, density profiles are opposite of each other in Figure 2b-c in the context of location of electrodes. Spatial and temporal density profile of electrons is governed by continuity Equation (10) coupled with other equations. Electron density grows to a level  $10^{11}/\text{cm}^3$ . Electrons respond to electric field very fast due to low mass and high mobility. There is deposition of electrons on the dielectric surface over grounded electrode during negative part of the cycle. Dielectric surface behaves as a negative electrode after negative peak of the rf voltage till the end of the cycle.

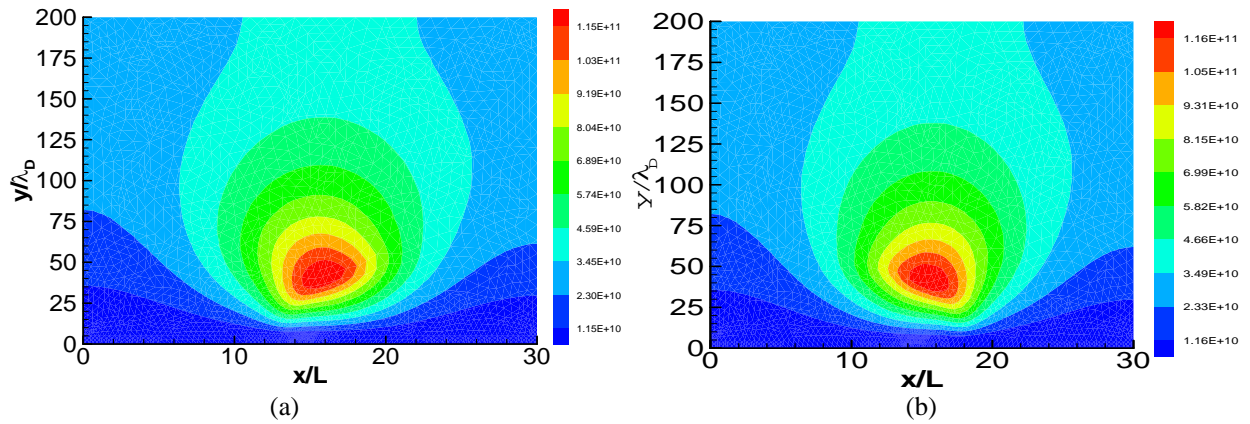


(a)



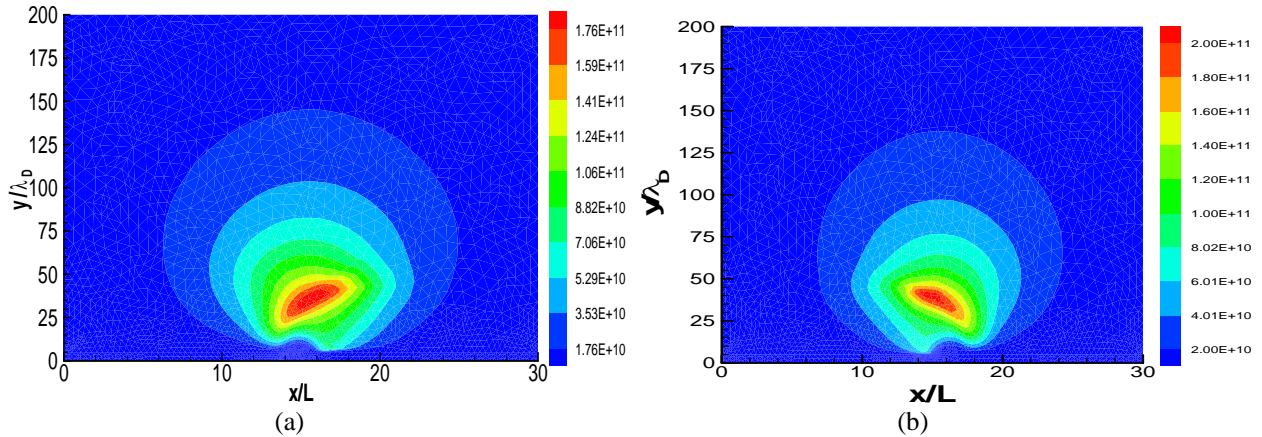
**FIG. 2. Evolution of electron density  $n_e$  (a) as a function of normalized time  $\omega t$  for  $x/L=15$  and  $y/\lambda_D=25$ , (b) at positive peak of the 20th cycle  $\omega t = 38.5\pi$ , and (c) at negative peak of the cycle  $\omega t = 39.5\pi$ .**

Initial density of the nitrogen atoms was taken zero. The nitrogen atoms are produced through dissociation. Chemistry of nitrogen atom formation is given by Equation (2) and its density is governed by continuity Equation (10) coupled with other equations. Density of nitrogen atoms grows to the same level as that of electrons, *i.e.*,  $10^{11}$  / $\text{cm}^3$ . Figure 3 shows distribution of nitrogen atom density at positive and negative peaks of the twentieth cycle. Since nitrogen atom do not have any charge, no electric force works on these atoms.



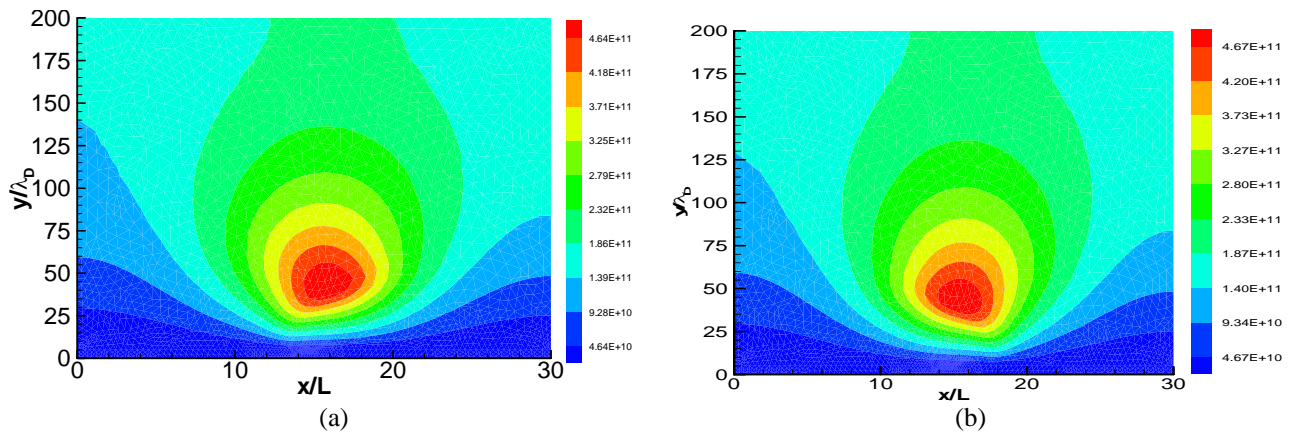
**FIG. 3. Distribution of nitrogen atoms N (a) at positive peak of the cycle  $\omega t = 38.5\pi$ , and (b) at negative peak of the cycle  $\omega t = 39.5\pi$ .**

Initial density of the nitrogen ions  $N_2^+$  was taken zero. The nitrogen ions  $N_2^+$  are produced through ionization of nitrogen molecules. Chemistry of nitrogen ions  $N_2^+$  formation is given by Equation (1) and its density is governed by continuity Equation (12) coupled with other equations. Density of nitrogen ions  $N_2^+$  grows to the same level as that of electrons, *i.e.*,  $10^{11}$  /cm<sup>3</sup>. Figure 4 shows distribution of nitrogen ions density  $n_{N_2^+}$  at positive and negative peaks of the twentieth cycle. The nitrogen ions  $N_2^+$  are repelled from the area of rf electrode and are attracted towards grounded electrode during positive part of the cycle. Reverse happens during negative part of the cycle, hence, density profiles are opposite of each other in Figure 4. Since positive ions respond to electric field in an opposite manner, density profiles are opposite to that of density profile of electrons in the context of location electrodes. The ions are much heavier than that of electrons; mobility of ions is low, the ions remain close to the wall than electrons.



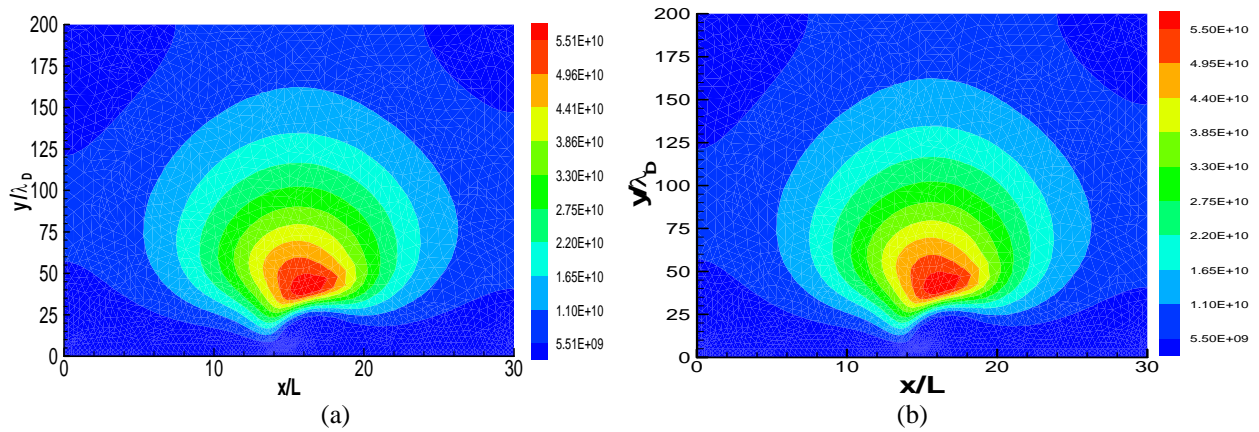
**FIG. 4. Distribution of nitrogen ions  $N_2^+$  density (a) at positive peak of the cycle  $\omega t = 38.5\pi$  , and (b) at negative peak of the cycle  $\omega t = 39.5\pi$  .**

Initial density of the oxygen atoms O was taken zero. The oxygen atoms are produced through dissociation of oxygen molecules. Chemistry of oxygen atoms formation is governed by Equation (5) and its density is governed by continuity Equation (14) coupled with other equations. Figure 5 shows density profile of oxygen atom O at positive peak of the cycle  $\omega t = 38.5\pi$  , and at negative peak of the cycle  $\omega t = 39.5\pi$  . Density of oxygen atoms is higher than that of nitrogen atoms due to difference in rate coefficients related to formation of nitrogen and oxygen atoms. Density profiles of both nitrogen and oxygen atoms are similar because both are neutral atoms and do not respond to electric field.



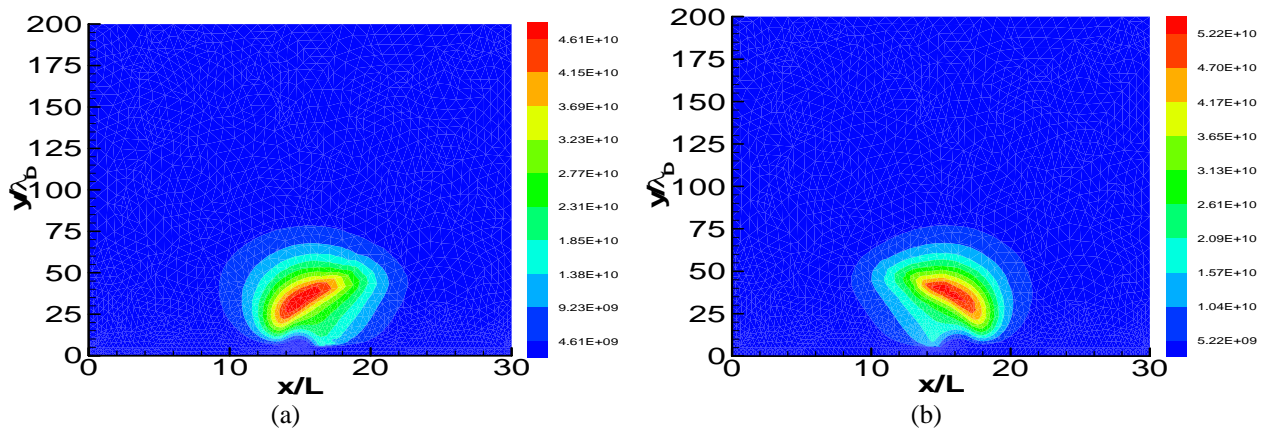
**FIG. 5. Distribution of oxygen atom O density (a) at positive peak of the cycle  $\omega t = 38.5\pi$  , and (b) at negative peak of the cycle  $\omega t = 39.5\pi$  .**

Initial density of the oxygen ions  $O^-$  was taken zero. The oxygen ions  $O^-$  are produced through dissociative attachment of oxygen molecules with electrons governed by Equation (6). Its density is governed by continuity Equation (15) coupled with other equations. Density of oxygen ions  $O^-$  grows to a level of slightly less than that of density of nitrogen ions  $N_2^+$ . Figure 6 shows distribution of density of oxygen ions  $O^-$  at positive and negative peaks of the twentieth cycle. The oxygen ions  $O^-$  are repelled from the area of grounded electrode and are attracted towards rf electrode during positive part of the cycle. Reverse happens during negative part of the cycle, hence, density profiles are opposite of each other in Figure 6. The oxygen ions  $O^-$  are much heavier than that of electrons and mobility is low; response is delayed. The ions remain close to the wall than electrons.



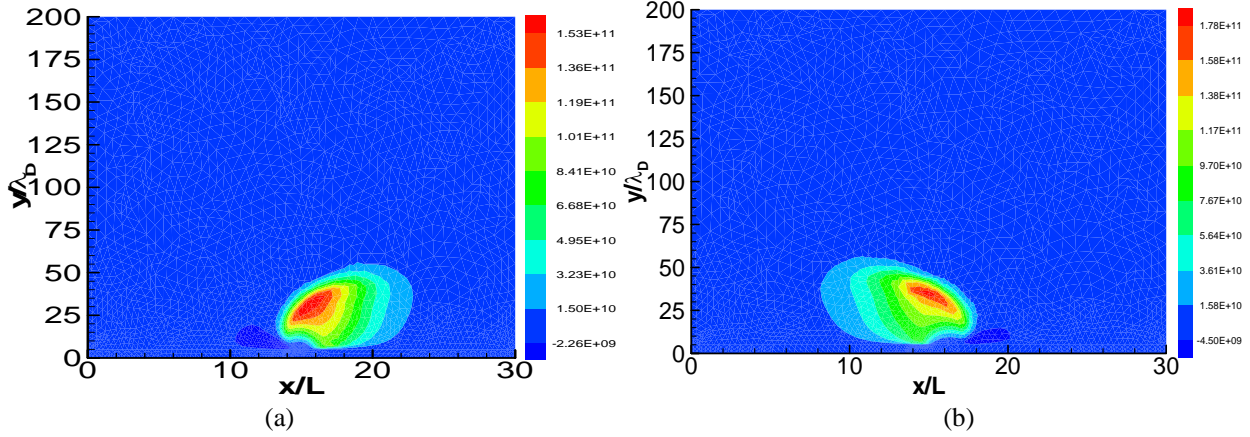
**FIG. 6. Distribution of negative oxygen ion  $O^-$  (a) at positive peak of the cycle  $\omega t = 38.5\pi$ , and (b) at negative peak of the cycle  $\omega t = 39.5\pi$ .**

Initial density of the oxygen ions  $O_2^+$  was taken zero. The oxygen ions  $O_2^+$  are produced through ionization of oxygen molecules. Chemistry of oxygen ions  $O_2^+$  formation is given by Equation (4) and its density is governed by continuity Equation (16) coupled with other equations. Density of oxygen ions  $O_2^+$  grows to the same level as that of  $O_2^+$  i.e.  $5 \times 10^{10} / \text{cm}^3$ . Figure 7 shows distribution of oxygen ions density  $O_2^+$  at positive and negative peaks of the twentieth cycle. The  $N_2^+$  and  $O_2^+$  respond to electric field in a similar manner, hence, their density profiles are similar to each other at same time instance. The difference between density levels of nitrogen and oxygen is because of ratio of these gases in atmospheric air.



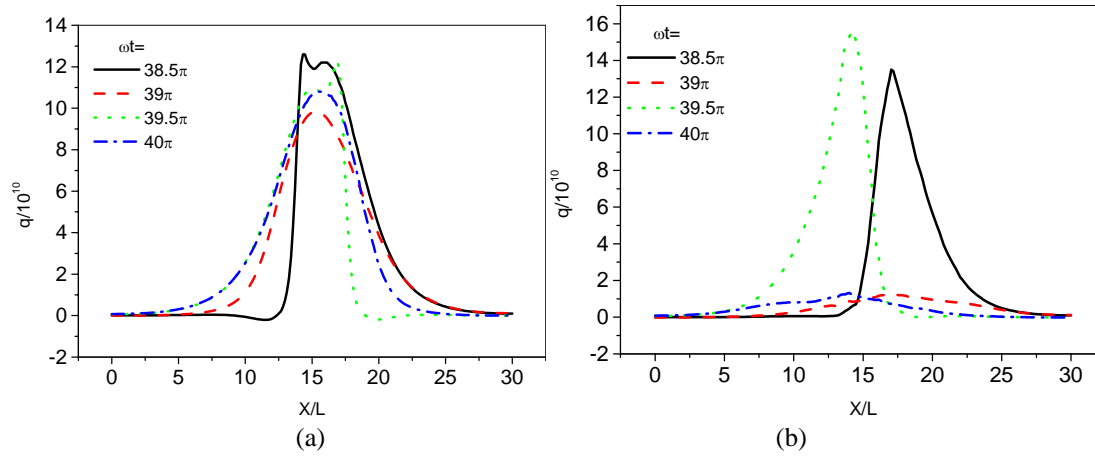
**FIG. 7. Distribution of positive oxygen ion  $O_2^+$  (a) at positive peak of the cycle  $\omega t = 38.5\pi$ , and (b) at negative peak of the cycle  $\omega t = 39.5\pi$ .**

Charged particles move in response to the electric field as described above. This give rise to charge separation  $q = e(n_{O_2^+} + n_{N_2^+} - n_e - n_{O^-})$ . Density profile of charge separation is shown in Figure 8. It resembles that of density profiles of positive nitrogen and oxygen ions. Level of charge separation matches density of  $N_2^+$  ions and electrons because densities of other charge species  $O^-$  and  $O_2^+$  is small in comparison. Charge separation gives rise to a self-generated electric field through Poisson's Equation.



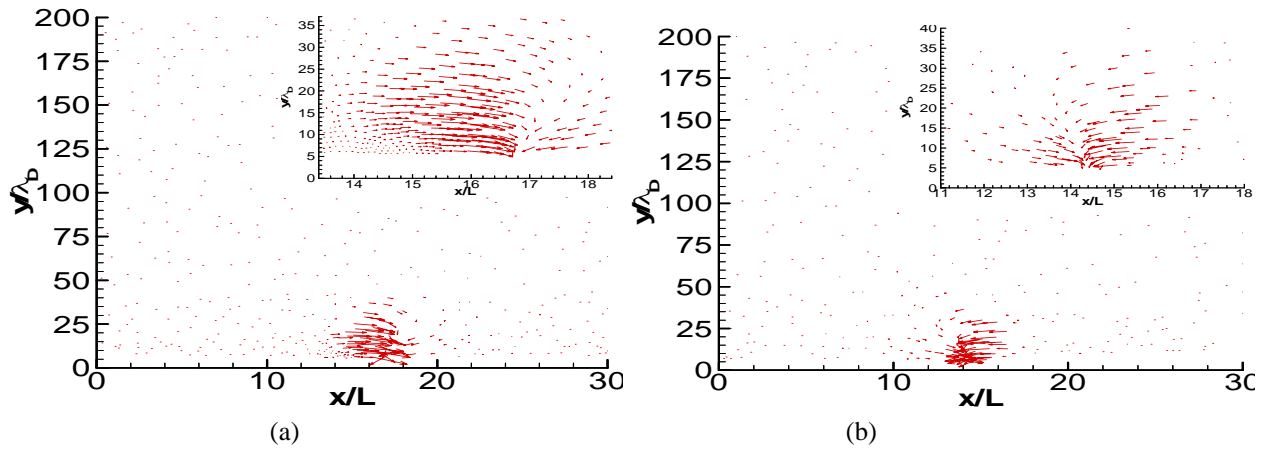
**FIG. 8. Distribution of charge separation  $q = e(n_{O_2^+} + n_{N_2^+} - n_e - n_{O^-})$  (a) at positive peak of the cycle  $\omega t = 38.5\pi$ , and (b) at negative peak of the cycle  $\omega t = 39.5\pi$ .**

Figure 9 shows charge separation  $q = e(n_{O_2^+} + n_{N_2^+} - n_e - n_{O^-})$  along the surface of dielectric at  $y/\lambda_D = 20$  and  $y/\lambda_D = 40$ . Charge separation is highest in the area of electrodes where discharge activity occurs. Charge separation is highest at voltage peaks of the cycle because of high electric field. Low electric field is associated with  $\omega t = 39\pi$  and  $40\pi$  for  $y/\lambda_D = 40$ , hence, charge separation is low at these points. We can also see that peak of charge separation moves towards higher value of  $y/\lambda_D$  at positive peak of the cycle. A small negative charge deposition is also noticed. These solutions are basic and needs to incorporate the effect of nitrous oxide and metastable species.



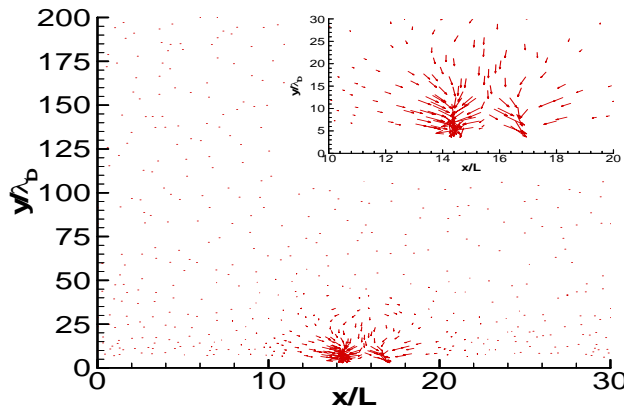
**Figure 9. Charge separation  $q$  as a function of normalized distance  $x/L$  for  $\omega t = 38.5\pi$ ,  $39\pi$ ,  $39.5\pi$  and  $40\pi$  at (a)  $y/\lambda_D = 20$  and (b)  $y/\lambda_D = 40$ .**

Electric field  $\mathbf{E}$  exerts a force  $\mathbf{F} = e(n_{N_2^+} + n_{O_2^+} - n_e - n_{O^-})\mathbf{E}$  on the charge separation. Figure 10 shows vectors of force distribution in the domain at positive and negative peaks of the twentieth cycle. The force is directed towards positive- $x$  direction at positive peak of the cycle and towards negative- $x$  direction at negative peak of the cycle. It is also directed towards wall at both the points of the cycle. The force follows direction of the electric field.



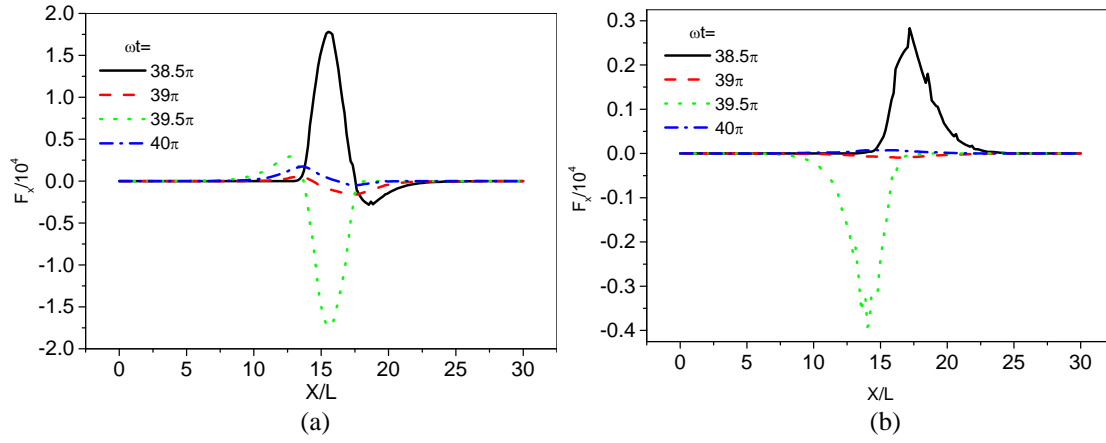
**FIG. 10. Vectors of force in the domain (a) at positive peak of the cycle  $\omega t = 38.5\pi$ , and (b) at negative peak of the cycle  $\omega t = 39.5\pi$ .**

Figure 11 shows time average of the force during twentieth cycle. The time average of the force is mostly directed towards negative y-direction with orientation towards positive x direction. The force lines are concentrated over the exposed and grounded electrodes. The electrons respond to the electric field very quickly due to high mobility. The electrons get deposited at the surface of the dielectric above grounded electrode during negative part of the cycle and the dielectric surface becomes negatively charged. It behaves as virtual negative electrode after negative peak of the cycle till the end of cycle. The peak magnitude of the force is located downstream of the rf electrode.



**FIG. 11. Vectors of time average of force distribution in the domain during a full cycle.  $x$  and  $y$  are in cm.**

The x-component of the force  $F_x = qE_x$  is shown in Figure 12 along the surface of dielectric at  $y/\lambda_D = 20$  and  $y/\lambda_D = 40$ . Magnitude of force is large at the peaks of the cycle. Most of the force is concentrated in the region of electrodes. The force is positive at positive peak of the cycle and negative at negative peak. The y-component of the force is mostly negative as shown in Figure 13. We can see again that force is highest at the peaks of the cycle and concentrated in the region of electrodes. At positive peak of cycle, peak of the force is at higher value of  $x/L$ . These results can be explained by considering direction and magnitude of the electric field. Direction of electric field is from rf electrode to grounded electrode at positive peak of the cycle and vice versa. Magnitude of electric field is highest at the peaks of cycle. Electric field decreases with distance from electrodes, hence, force also decreases.



**Figure 12. x-component of the force  $F_x$  as a function of normalized distance  $x/L$  for  $\omega t = 38.5\pi$ ,  $39\pi$ ,  $39.5\pi$  and  $40\pi$  at (a)  $y/\lambda_D=20$  and (b)  $y/\lambda_D=40$ .**

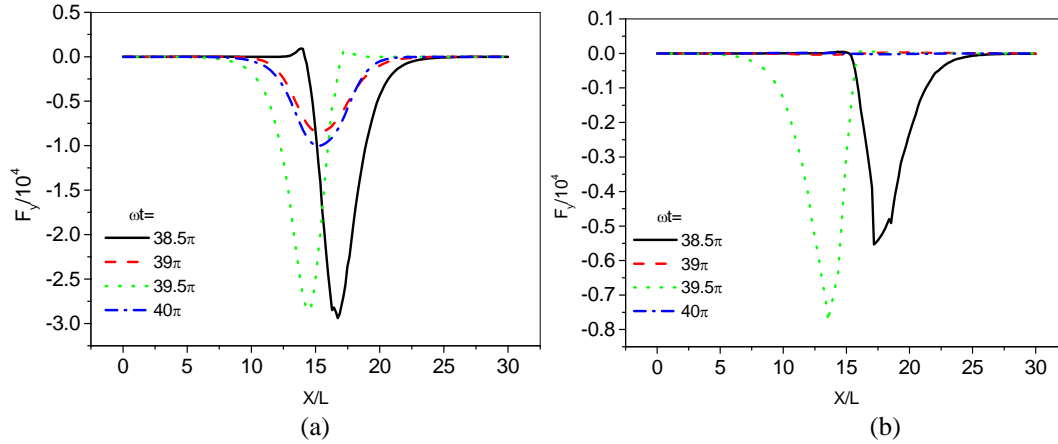


**Figure 13. y-component of the force  $F_y$  as a function of normalized distance  $x/L$  for  $\omega t = 38.5\pi$ ,  $39\pi$ ,  $39.5\pi$  and  $40\pi$  at (a)  $y/\lambda_D=20$  and (b)  $y/\lambda_D=40$ .**

#### IV. Conclusions

Air discharge has been studied using an asymmetric dielectric barrier plasma actuator. A self-consistent plasma actuator model is employed to study surface discharge of air. Chemistry of formation of different ion and neutral species of nitrogen and oxygen has been taken into account. Species with very high recombination rates and nitrous oxide have been neglected for simplicity. Continuity equations governing densities of electrons, ions and neutral species of nitrogen and oxygen are solved with Poisson's equation using a two-dimensional finite element based formulation of plasma to obtain spatial and temporal profiles of densities, and voltage. Poisson's equation governs electric field generated due to charge separation. Computed results show that for this simplistic model oppositely charged species move in opposite directions due to applied driver rf potential. Response of electrons to electric field is very fast as compared to ions due to small mass and high mobility of electrons. Density profiles of different species are nearly opposite to each other at positive and negative peaks of the cycle. Density profiles of nitrogen atom N and oxygen atom O are similar because these do not move due to electric field. Density profiles of  $N_2^+$  and  $O_2^+$  are similar to each other at any specific time instance because they respond to electric field in a similar manner. There is, however, difference in level of ionization of different species due to difference in rate coefficients. The motion of electrons and ions results in charge separation. Electron deposition downstream of the overlap region of the electrodes during negative part of the cycle results in formation of virtual negative electrode. The value of charge separation  $q = e(n_{O_2^+} + n_{N_2^+} - n_e - n_{O^-})$ , and the electrodynamic force per volume  $\mathbf{F} = e(n_{N_2^+} + n_{O_2^+} - n_e - n_{O^-})\mathbf{E}$  have been obtained near the dielectric surface for twentieth cycle. Time average of the x-force is positive and y-force is negative over the domain, therefore, there is an

average net force on the plasma in positive  $x$  and negative- $y$  direction. This will result in a moving wave of plasma over the dielectric surface in positive  $x$ -direction which can find application in flow control. A detail air chemistry model with Poisson-Navier-Stokes equations is also under development for exploration of the effect of a plasma actuator operating in air using realistic geometry and electrode configurations. In this model, an in-depth study involving more species like NO will be incorporated to investigate the effect of surface air discharge and its coupling with the neutral gas flow.

### Acknowledgements

The work is partially supported by Air Force Research Laboratory contracts and the AFOSR grant with Technical Monitors Dr. John Schmisser and Lt. Col. Rhett Jefferies. The authors acknowledge many thoughtful discussions about air chemistry with Mr. Eswar Josyula.

### References

- <sup>1</sup> K.W. Van Treuren, *et al.* J. Turbomachinery **124**, 100 (2002).
- <sup>2</sup> J.P. Bons, R. Sondergard and R.B. Rivir, J. Turbomachinery **123**, 198 (2001).
- <sup>3</sup> J. R. Roth and X. Dai, 2006, AIAA-2006-2103.
- <sup>4</sup> J. Pons, E. Moreau and G. Touchard 2005 J. Phys. D: Appl. Phys. **38**, 3635–3642.
- <sup>5</sup> S. Roy, Appl. Phys. Lett. **86**, 101502 (2005); S. Roy, K.P. Singh and D. Gaitonde, Appl. Phys. Lett. **88**, 121501 (2006).
- <sup>6</sup> K.P. Singh and S. Roy, J. Appl. Phys. **98**, 083303 (2005).
- <sup>7</sup> Y. B. Suzen, P. G. Huang, J. D. Jacob and D. E. Ashpis, 2005, AIAA-2005-4633, June.
- <sup>8</sup> Gabriel I. Font and W. Lowell Morgan, 2005, AIAA-2005-4632, June.
- <sup>9</sup> E. Josyula and W.F. Bailey, Journal of spacecrafts and Rockets, **40**, 845 (2003).
- <sup>10</sup> I. A. Kossyi, A. Yu Kostinsky, A.A. Matveyev and V.P. Silakov, Plasma Sources Sci. Techol., **1**, 207 (1992).
- <sup>11</sup> M. Forte, L. Leger, J. Pons, E. Moreau and G. Touchard 2005 J. Electrostatics **63**, 929-936.
- <sup>12</sup> S. Roy, K.P. Singh, H. Kumar, D.V. Gaitonde and M.R. Visbal, 2006, AIAA-2006-0374, January.
- <sup>13</sup> J. P. Boeuf and L. C. Pitchford, J. Appl. Phys. **97** 103307 (2005).
- <sup>14</sup> D.V. Gaitonde, M.R. Visbal and Subrata Roy, AIAA-2005-5302, 36th AIAA Plasmadynamics and laser coferance, June 2005, Toronto, Canada.
- <sup>15</sup> M. Visbal, D. Gaitonde, and S. Roy, 2006. AIAA-2006-3230, June.
- <sup>16</sup> D.V. Gaitonde, M.R. Visbal and S. Roy, 2006, FEDSM2006-98553, ASME Joint U.S. - European Fluids Engineering Summer Meeting.
- <sup>17</sup> H.W. Ellis, R.Y. Pai, E.W. McDaniel, E.A. Mason, and L.A. Viehland, Atomic Data Nucl. Data Tables, **17**, 177, 1976.
- <sup>18</sup> S. Roy, et al., Phys. Plasmas, **10**, 2578 (2003); S. Roy and D. Gaitonde, Phys. Plasmas, **13**, 023503 (2006).